5.1 INTRODUCTION

The wear and erosion behavior of AM parts have been major concerns in various applications in recent times and their performance in comparison to the functionality of parts made using conventional materials is actively being explored. In this study, the wear and erosion behavior of additively manufactured maraging steel with three different build orientations (0^o, 45^o, and 90^o) were investigated and compared with those of conventional manufactured (cast and hot rolled) steel samples. The aim of this study is to provide a comprehensive understanding of the wear and erosion behavior of additively manufactured maraging steel and to explore the potential of this technology in producing wear and erosion resistant components.

As-built and heat-treated maraging steel samples were wear-tested at various loads of 20N, 40N and 80N, at a constant disc speed and for a specific sliding distance. Erosion tests were performed at a 90^o impingement angle for 40 minutes at an erosion discharge rate of 4.5 g/min. The wear and erosion rates were calculated and the tested samples were examined under scanning electron microscopy (SEM) and atomic force microscopy (AFM). The present study provides valuable insights into the wear and erosion behavior of additively manufactured maraging steel and highlights its potential as a wear-resistant material in various applications. These findings can help in the selection of appropriate build orientation and heat treatment parameters for producing wear and erosion resistant components using AM technology.

5.2 Wear and Erosion Behaviour

5.2.1 Microstructural Characterization

The faces, of the samples subjected to rubbing action against rotating disc in the wear test, are denoted as 0^o AB_w, 45^o AB_w and 90^o AB_w in Fig. 5.1(a). The faces on which the

high velocity erosion particles fall in erosion test are denoted as 0^o AB_E, 45^o AB_E and 90^o AB_E in Fig. 5.1 (b).

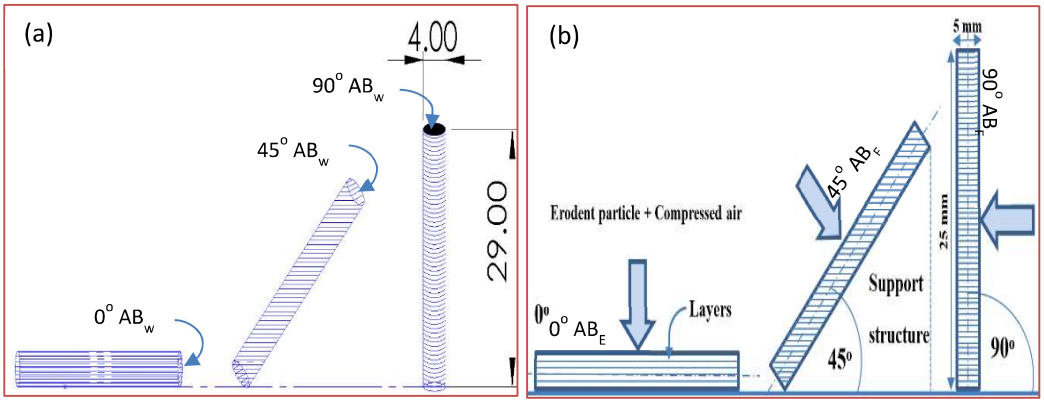

Fig. 5.1 Schematic presentation of 0^o, 45^o and 90^o built samples used for: (a) wear test sample, 0^0 AB_w, 45^o AB_w and 90^o AB_w are mating surfaces with rotating disc and (b) erosion test samples, 0^0 AB_w, 45^o AB_w and 90^o AB_w are exposed surfaces in erosion.

The microstructures of the faces involved in wear study in the as built condition are shown in Figs. 5.2 (a, b, c and d). Similarly, the microstructures of the faces involved in erosion testing have been shown in Figs. 5.2 (a', b', c' and d').

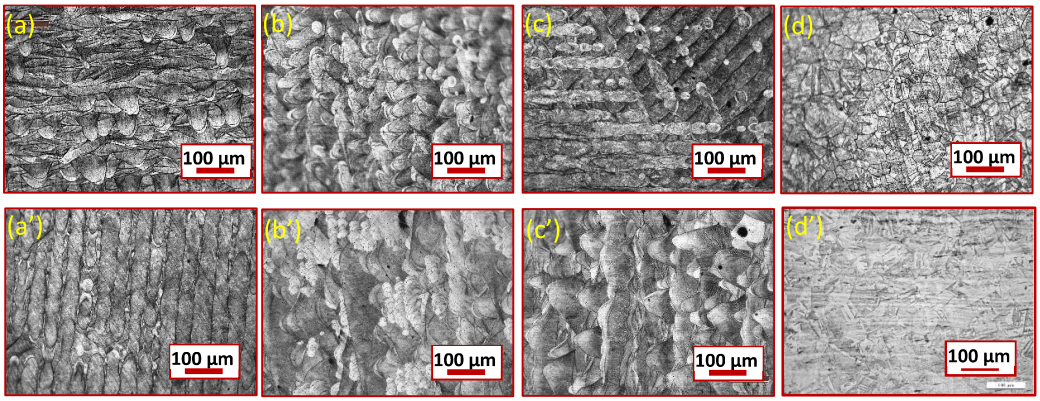

Fig. 5.2 Microstructure of the as built samples in 0^o, 45^o, 90^o orientation and conventional samples taken from the faces of wear and erosion testing: (a) 0^o AB_w (b) 45^o AB_w (c) 90^o AB_w and (d) CM_w (a') 0^o AB_E (b') 45^o AB_E (c') 90^o AB_E. and (d') CM_E.

Both wear and erosion tested faces of the conventional samples showed similar microstructure, and are represented in Figs. 5.2 (d and d'). The as-built additive samples

depicted different features at various magnifications. At low magnification, process characteristics like layers, laser tracks and melt pool can be seen. Fig. 5.2 (a) shows the 0^o AB_w face depicting meso-structure, with stacking of overlapped layers of thickness ~30 μm and semi-elliptical melt pool of size ~70 μm. Fig. 5.2 (b) presents the meso-structure in 45^o AB_w sample showing the end region of 67^o oriented laser scan. Fig. 5.2 (c) shows 90^o AB_w face meso-structure of laser scanned regions with 67^o inter-layer rotation. Similarly, the exposed faces from erosion samples, Fig.2.6 (b) from as-built plates in 0^o, 45^o and 90^o build orientations were taken for microstructural characterization. Fig. 5.2 (a') shows 0^o AB_E face exposed for erosion, which depicts laser tracks of spot diameter of around 60 μm. Fig. 5.2 (b') shows the 45^o AB_E face in which overlapped layers can be seen. Fig. 5.2 (c') shows 90^o AB_E surface exhibiting stacking of layers with melt pool characteristics. Figs. 5.2 (d and d') present the microstructure of as received conventional samples taken for wear and erosion studies, showing equiaxed grains of size ~ 40 μm.

At higher magnification, the as-built additive samples of all orientations show mainly fine cellular and columnar grains. The columnar grains nucleate from the melt pool boundary and grow towards the centre of the melt pool. Considering laser tracks, seeing from the top (laser scanning side, Figs. 5.2 (c and a') show the cellular grains (end view of columnar grains) and while observing from the side [Figs. 5.2 (a, b, b' and c')], the columnar grains can be seen. The SLM processing consists of complex heating and cooling cycles due to which mixed type of grains are observed on all faces. Fig. 5.3(a) shows the high magnification optical micrograph of laser tracks; which is common in laser scan faces i.e. [Figs. 5.2 (c, a')], mainly depicts fine cellular grains (< 1 μm). Fig. 5.3(c) shows a magnified view of the highlighted region of Fig. 5.3(a). Fig. 5.3(b) shows the high magnification optical micrograph from the transverse side which is common for

Fig. 5.2(a, b, b' and c'), where melt pool characteristics exist. It shows mainly columnar grains with some cellular grains. At the base of the melt pool, mainly columnar grains were observed while away from the junction of two layers, cellular grains were observed. Fig. 5.3(d) shows a magnified view of the highlighted region of Fig. 5.3(b).

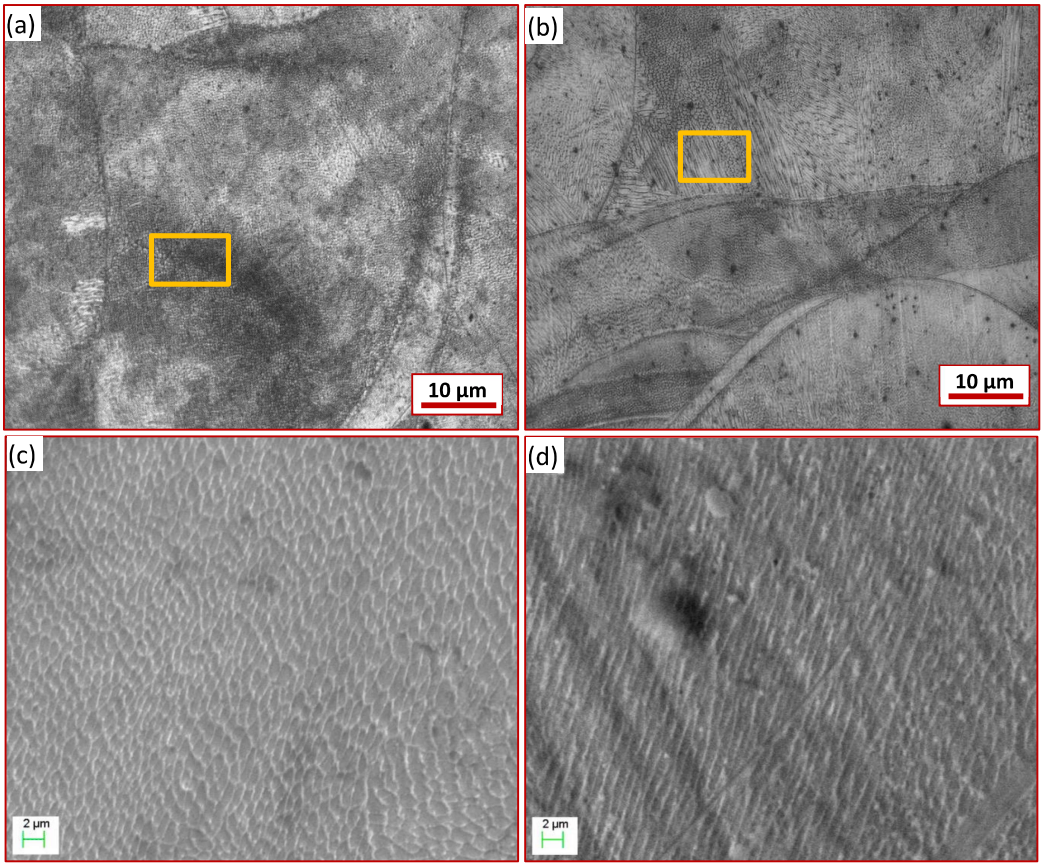

Fig. 5.3 Optical micrographs of 0° as-built samples at higher magnification (a) laser scanning side (b) layers or melt pool side (c) micrograph at higher magnification of selected region in (a) and (d) micrograph at higher magnification at selected region in (b).

After heat treatment, all the above-mentioned features resulting due to AM processing disappeared and fine lath martensite structure was observed. The heat-treated additive samples showed similar microstructure for all orientations (0°, 45° and 90°). Fig. 5.4(a) shows heat treated micrograph of 0° HT additive samples which depicts very fine lath

martensite. Fig. 5.4(b) presents a micrograph of conventional heat treated (CHT) sample, showing coarser lath martensite structure.

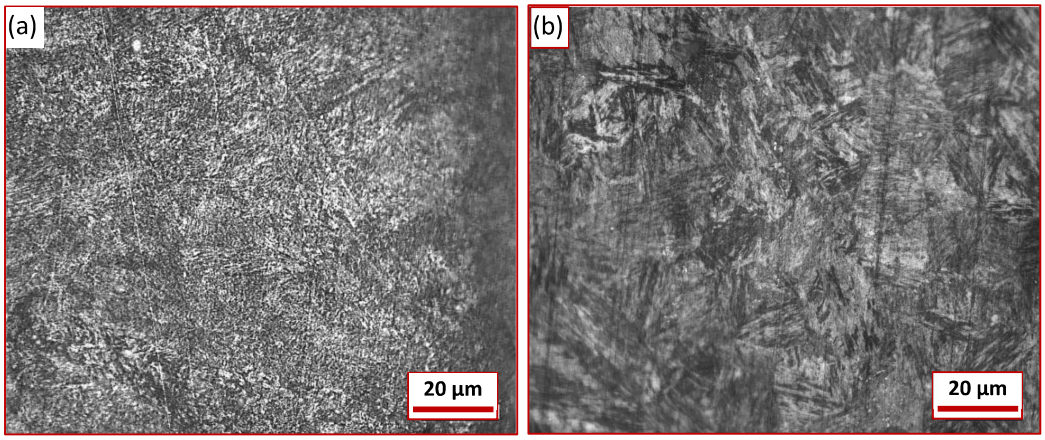

Fig. 5.4. Optical micrographs of heat-treated samples: (a) additive sample in 0^{o} orientation showing very fine lath martensite (b) conventional sample showing coarser lath martensite.

5.2.2 Wear rate

Figs. 5.5 (a and, b) present the variation of wear rate of the AM samples in the as-built and heat-treated conditions, at varying loads and built orientations, along with those observed in the conventional samples. It can be observed that firstly wear rate increases in a linear fashion, gradually retards and becomes constant at higher load in the as-built/as-received conditions while in the HT samples, increase in the rate of wear, up to load of 80 N, can be observed as shown in Fig. 5.5(b).

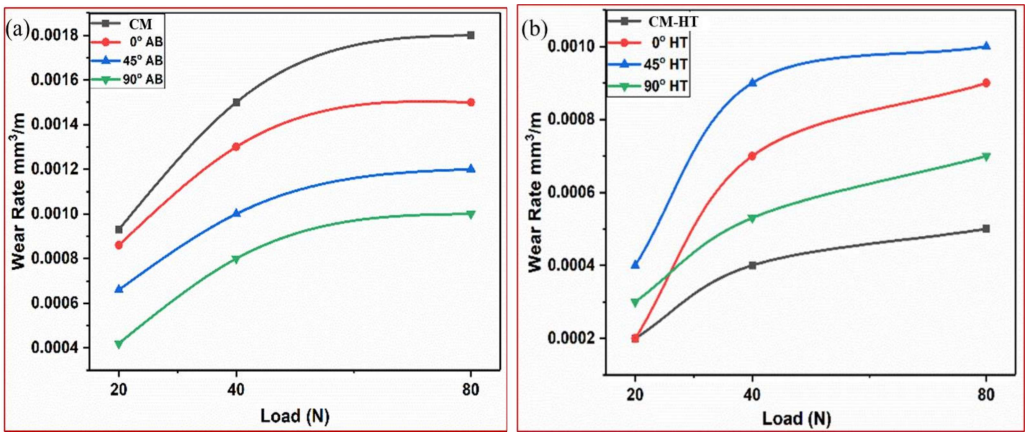

Fig. 5.5 Variation of wear rate as a function of applied load in specimens: (a) conventional as received (CM) and additive samples as-built (AB) in 0°, 45° and 90° orientations and (b) conventional heat treated (CM-HT) and additive manufactured in 0°, 45° and 90° orientations followed by heat treated (HT) conditions.

The wear rates of all the conditions are recorded in Table. 5.1. Wear rate of the as-built samples was found to decrease with increase in build orientation. Maximum wear rate was observed in conventionally processed material in as received condition in comparison to those of the additive samples in the as-built state. Wear rate at 80 N was found to be in the following order: CM (0.0018 mm^3/m) > 0° AB (0.0015 mm^3/m) > 45° AB (0.0012 mm^3/m) > 90° AB (0.001 mm^3/m). After heat treatment, maximum wear rate was observed in 45° HT samples and was followed by 0° HT, 90° HT and CM-HT samples, respectively. The order of wear rate for heat-treated samples at 80 N can be expressed as: 45° HT (0.0010 mm^3/m) > 0° HT (0.0009 mm^3/m) > 90° HT (0.0007 mm^3/m) > CM-HT (0.0005 mm^3/m).

Table. 5.1 Wear rates observed in conventional and additive samples in as-built and heat-treated conditions.

Load, N	Wear Rate, mm^3/m (in 10^{-3})							
	CM	CM-HT	0° AB	0° HT	45° AB	45° HT	90° AB	90° HT
20	0.9	0.2	0.8	0.2	0.6	0.4	0.4	0.3
40	1.5	0.4	1.3	0.7	1.0	0.9	0.8	0.4
80	1.8	0.5	1.5	0.9	1.2	1.0	1.0	0.7

5.2.3 Coefficient of friction (COF)

Figs 5.6(a and b), show variation in average wear coefficient of additive and conventionally processed samples with load in as-built and heat-treated conditions. The variation of COF in different conditions is presented in Table. 5.2. From Fig. 5.6(a), it can be noted that, as the applied load increased from 20 N to 80 N, wear coefficient was considerably decreased.

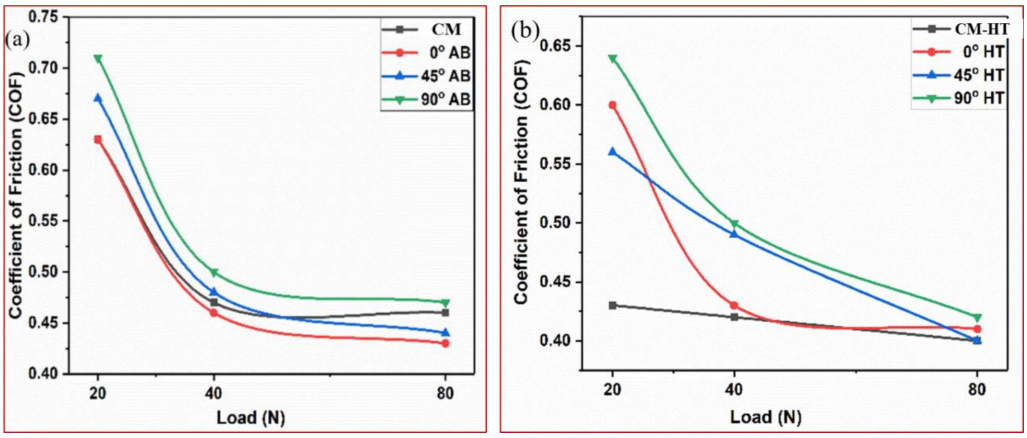

Fig. 5.6 Coefficient of friction (COF) vs load plots: (a) conventional as received (CM) and additive manufactured as-built (AB) in 0°, 45° and 90° orientations and (b) conventional heat treated (CM-HT) and additive manufactured in 0°, 45° and 90° orientations followed by heat treated (HT) conditions.

Table. 5.2 Coefficient of friction for conventional and additive samples in as-built and heat-treated conditions.

Load N	Coefficient of Friction (COF)							
	CM	CM-HT	0° AB	0° HT	45° AB	45° HT	90° AB	90° HT
20	0.63	0.43	0.63	0.60	0.67	0.56	0.71	0.64
40	0.47	0.42	0.46	0.42	0.48	0.49	0.50	0.50
80	0.46	0.40	0.43	0.43	0.44	0.40	0.47	0.42

Around 45% decrease in COF was observed in the as-built sample. Similarly, Fig. 5.6(b) shows that COF decreased with increase in applied load after heat treatment. At 20 N load, maximum value of COF is observed for 90° AB specimen (0.71), and followed by 45° AB (0.67), 0° AB (0.63) and CAR (0.63) respectively. Similarly, the COF in the HT sample at 20 N follows a trend, 90° HT (0.64) > 0° HT (0.60) > 45° HT (0.56) > CM-HT (0.43). Thus, it is clear that after heat treatment, the COF of the as-built samples was decreased. It can be concluded from Fig. 5.7 that during the initial stages, there was rapid rise in the COF and after that steady state with fluctuation in the COF curves as a function of time can be seen.

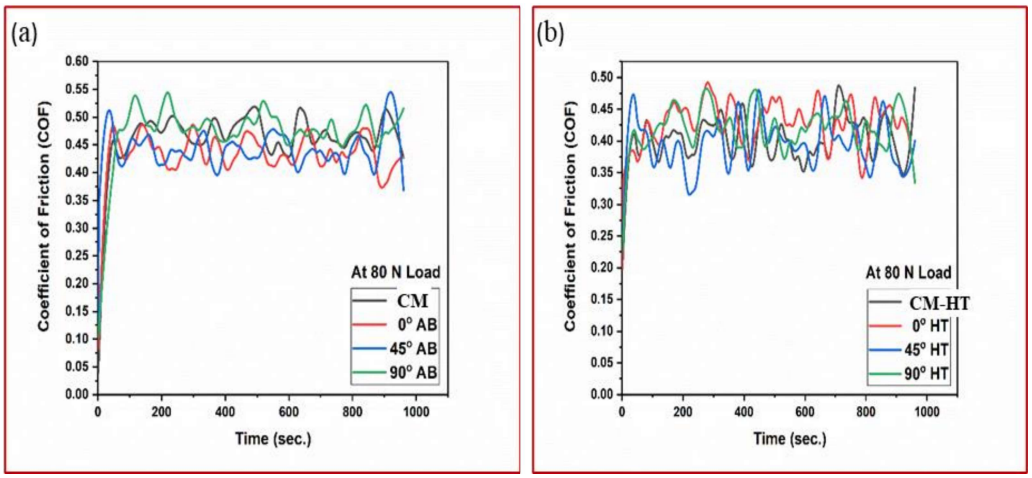

Fig. 5.7 Variation of coefficient of friction with time at 80 N load: (a) as built (AB) and Conventional as received (CM) specimen, (b) conventional heat treated (CM-HT) and additive manufactured followed by heat treated (HT) specimen

5.2.4 Erosion Rate

Mass loss of material, up to 4 decimal points, was noted and erosion rate was calculated using Eq. 2.8 given in Chapter 2. Fig. 5.8 shows comparison of erosion rate of the as-built and heat-treated samples in 0°, 45° and 90° orientations with the rates observed in conventional sample in the as received and heat-treated conditions. The conventional sample, in as received condition, exhibited more erosion rate than the rates in as-built additive samples. The erosion rate before heat treatment follows the trend: CM (1.37×10^{-4} gg^{-1}) > 90° AB (1.36×10^{-4}) > 45° AB (1.28×10^{-4}) > 0° AB (1.15×10^{-4}). After the heat treatment, the erosion resistance was improved and minimum erosion rate was observed for the 0° HT (8.3×10^{-5}) sample and was followed by 90° HT (1.01×10^{-4}), 45° HT (1.14×10^{-4}) and CM-HT (1.17×10^{-4}) samples respectively.

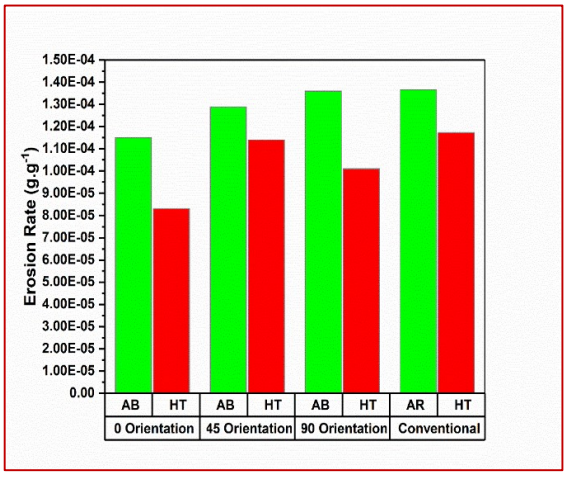

Fig. 5.8 Erosion rate of additive and conventional samples in as built/as-received and heat-treated conditions.

5.2.5 Morphology of worn surfaces

The worn surfaces tested at 20N load, are shown in Figs. 5.9(a, b, c and d) in conventional as received (CM) and additive samples in 0°, 45° and 90° build orientation. It is clear that

worn surfaces primarily consist of parallel deep grooves in all orientations as well as in the conventional samples. Figs. 5.9(a', b', c' and d') show the corresponding 3D profile images. Along with the clear wear tracks, wear debris was also observed as shown in Figs. 5.9(b, c, and d). By Comparing the 3D profiles at 20 N load, it can be inferred that as the build orientation increased from 0° to 90°, the width and depth of grooves decreased. The 0° AB sample shows groves width (~20 µm) and depth of about ±1 µm. Similarly, 45° AB and 90° AB samples show grooves width of ~15 µm and depth of about ±0.5 µm which support the results of wear rate and hardness. The worn surfaces were found to be smoother for the conventional and 0° AB samples and became coarser in 45° and 90° AB samples at 20N load. The aforementioned surface observations are in line with the results observed in the case of coefficient of friction at 20N load for the as-built samples.

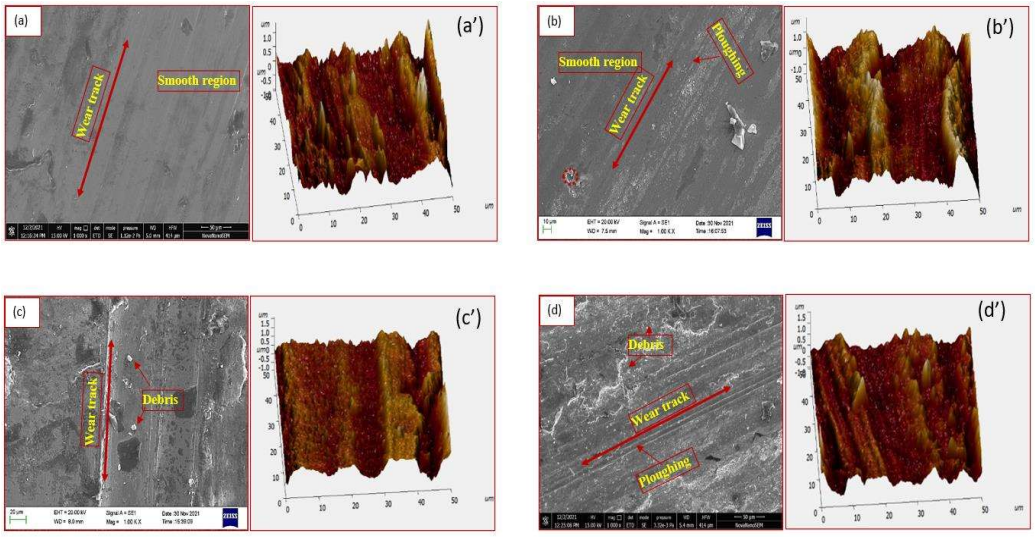

Fig. 5.9 Worn surfaces of as received conventional sample (CM) and as-built additive samples (AB) in different orientations at 20N load: (a) CM (b) 0° AB (c) 45° AB and (d) 90° AB and their corresponding 3D profile images (a', b', c' and d').

Surface morphology of the as-built/as-received additive and conventional samples, wear-tested at the highest load of 80 N is shown in Fig. 5.10. Fig. 5.10(a) shows the worn

surface of the CM samples; it depicts wear tracks as well as delamination. Similarly, worn surfaces of the as-built additive samples in Figs. 5.10(b, c, and d) show mainly materials transfer, delamination and plastic deformation on the surface. Smoother surface was observed for the 0^o orientation, followed by 45^o and 90^o AB samples and the results are consistent with the COF results of the respective samples. The 3D profiles of the samples tested at 80N, (Figs. 5.10 a', b', c' and d') reflect that only the conventional as received samples showed mixed wear characteristics, like wear tracks and delamination with a track width of about ~10 µm and peak and valley depth of ±300 nm. The 0^o, 45^o and 90^o AB samples showed only delamination and materials transfer, due to which there were no clear tracks and track width observed was ~200 nm as unevenness was created by materials transfer and delamination (Figs. 5.10 b', c' and d').

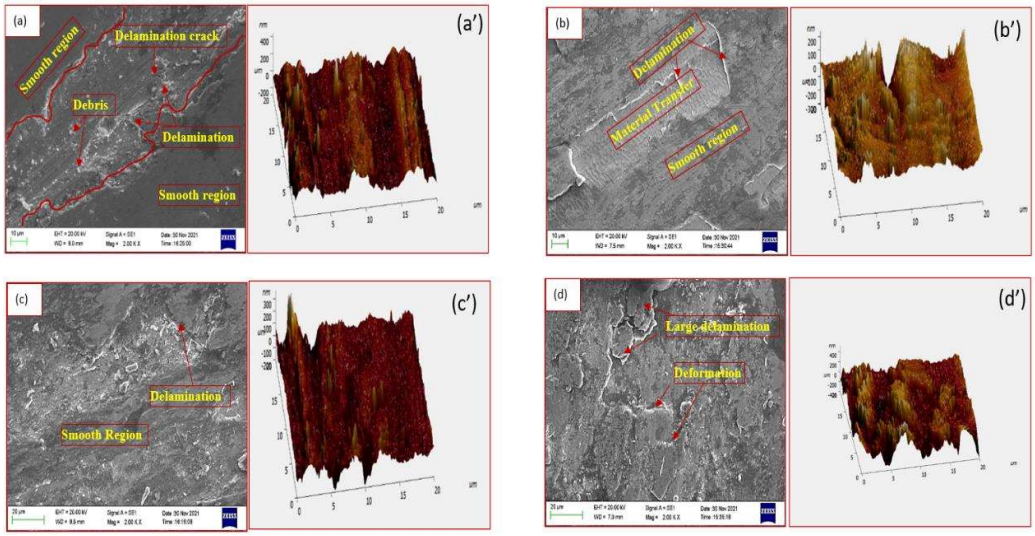

Fig. 5.10 Worn surfaces of as received conventional sample (CM) and as-built additive samples (AB) in different orientations at 80 N load: (a) CM (b) 0^o AB (c) 45^o AB and (d) 90^o AB and their corresponding 3D profile images (a', b', c' and d').

The wear surface morphology of heat-treated samples at highest applied load of 80 N displayed in Fig. 5.11(a, b, c and d).

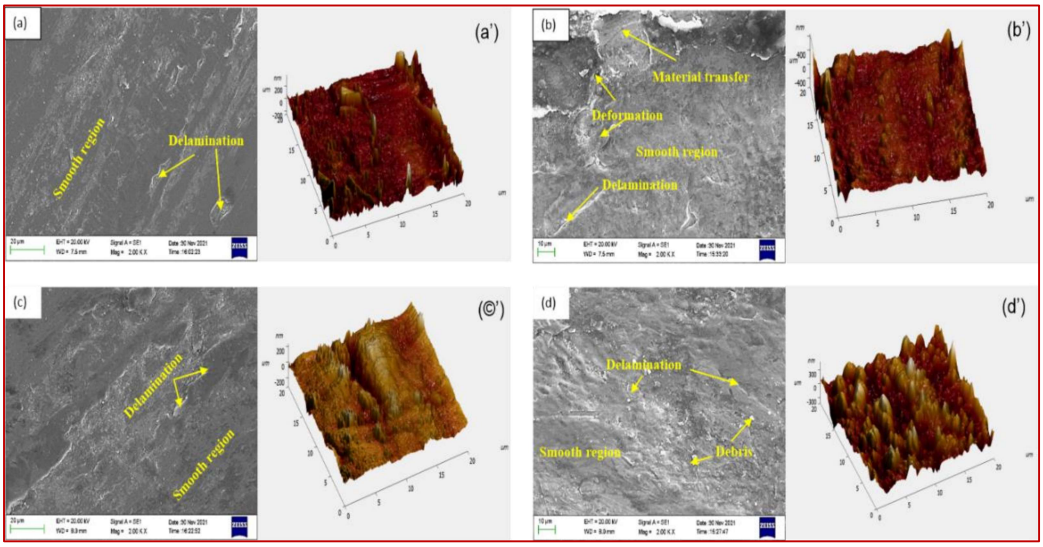

Fig. 5.11 Worn surfaces of heat-treated conventional and additive samples in different orientations: (a) CM-HT (b) 0° HT (c) 45° HT (d) 90° HT and their corresponding 3D profile images (a', b', c' and d').

Delamination and deformation were observed on worn surfaces of the conventional, 0°, 45° and 90° heat-treated samples. Smoother region was observed as compared to the surfaces of AB/CM wear tested samples at 80N applied load. The SEM observations of worn surfaces for the heat-treated samples were found to be matching with the COF and wear rate results of the respective samples.

5.2.6. Morphology of Eroded Surfaces

To identify the erosion behaviour and form of material loss of as-built and heat-treated samples during erosion process, eroded surface morphology was examined using SEM and are presented in Figs. 5.12 and 5.13.

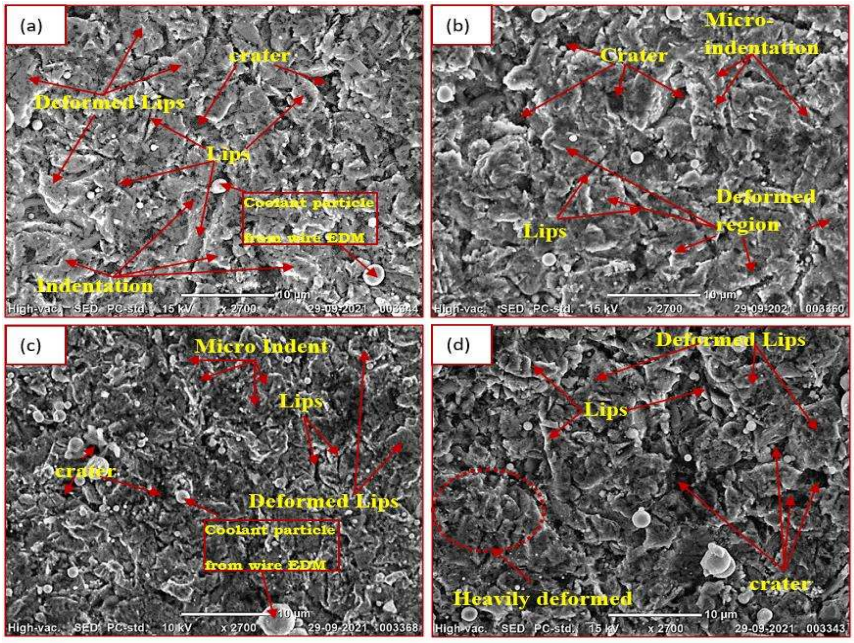

Fig. 5.12 Eroded surfaces of as-built (AB) additive samples in different orientations and conventional as received (CM) sample: (a) 0^o AB (b) 45^o AB (c) 90^o AB and (d) CM

Figs. 5.12(a and b) show eroded surfaces of 0^o AB and 45^o AB samples. Lip formation due to normal impact of erodent particles can be observed with deformed lips and indentation marks. Fig. 5.12(c) presents the surface of the 90^o AB sample after erosion. It shows comparatively smaller indentation marks and lips among the all-built orientations. Fig. 5.12(d) presents SEM image of eroded surface of CM sample and depicts larger crater size and heavily deformed region than those of the as-built samples built in different orientations. In all the eroded surfaces, shiny spherical particles can be observed, which are coolant particles remained after wire EDM cutting of the samples. After wire EDM, the samples were ultrasonically cleaned to remove these coolant particles to maximum extent. Eroded surfaces of the heat-treated samples, shown in Figs. 5.13(a, b, c and d), are similar to those observed for the AB/CM additive and conventional samples.

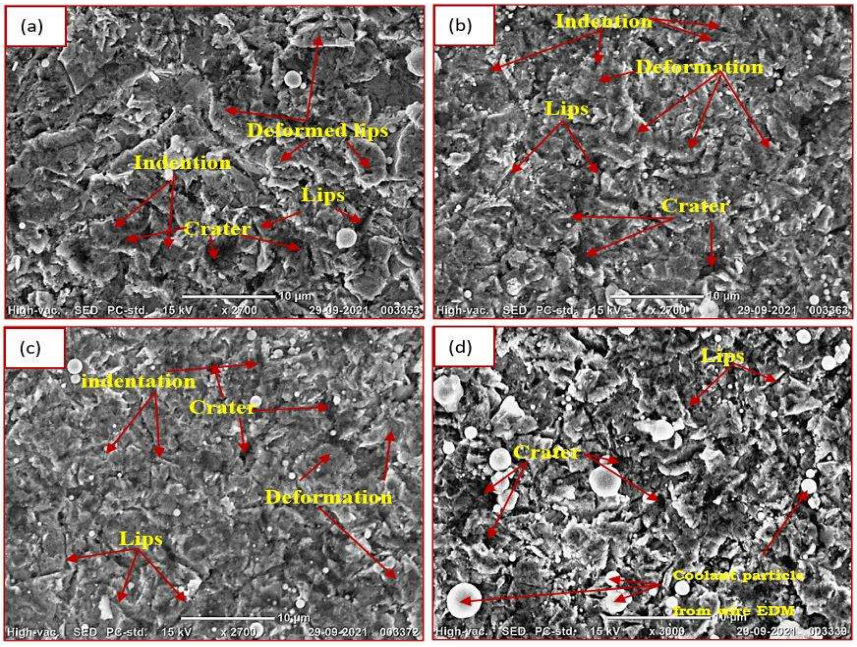

Fig. 5.13 Eroded surfaces of heat treated additive samples in different variations and conventional sample: (a) 0^{o} HT (b) 45^{o} HT (c) 90^{o} HT and (d) CM-HT

Fig. 5.14(a) shows plastic deformation on eroded samples with dimples. Further, magnified micrograph of Fig. 5.14(b) shows substrate material structure in the as built condition. From the analysis of Figs. 5.14(a and b), it is clear that erosion craters became the main morphology after erosion. In addition, many fragments of erosion particles can be observed in the craters. The side view of eroded samples shown in Fig. 5.14(c) displays a shallow contour profile of central depth of about 600 μm. The central region of eroded profile was magnified and is shown in Fig. 5.14(d) which shows indentation marks of erodent particles.

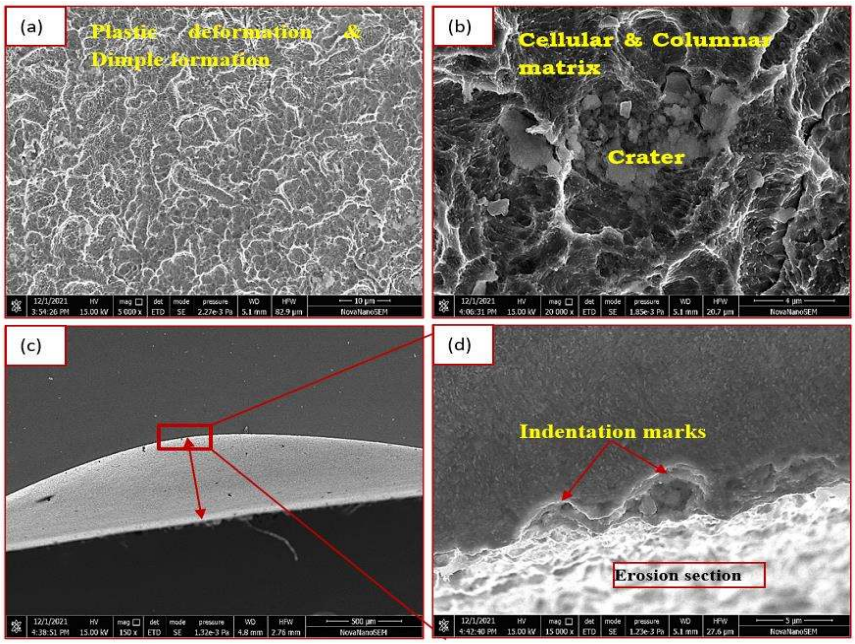

Fig. 5.14 (a) SEM micrograph of eroded surface (b) cellular and columnar microstructure in the as-built samples (c) cross-sectional view of eroded sample and (d) high magnification image of (c).

5.3 Discussion

5.3.1 Microstructure

The mating faces of samples showed different meso-structure (Fig. 5.2), viewed from different faces and angles. Meso-structure refers to the structure visible due to laser processing of powder layer by layer. During AM, materials undergo complex heating cycles, hence AM process leads to metastable microstructure [149]. The heat transfer rate in AM is about 10^7 K/s whereas in casting route, it is about 10^3 K/s, due to which AM materials do not get enough time for grain coarsening, hence the AM sample showed very fine microstructure as displayed in Fig.5.3, while the conventional samples showed large equiaxed grains (Fig. 5.2(d and d')) [150]. Heat conduction in build direction is typically higher than in the other spatial directions (x, y), as a result the solidified material from lower, previously built layers, shows anisotropy in microstructure in selected cases

as shown in Figs. 5.3(c and d) [151]. The columnar grains start from base of melt pool and approach towards the centre of the laser tracks, as a result, mostly columnar grains were observed [Fig. 5.3(b, d)], while observing from layer side (melt pool side). However, on visual examination from top (laser hatching faces), fine cellular grains were observed as shown in Fig. 5.3(a, c). The solution treatment temperature selected was 815^{o} C for 1h, which is on the lower side of solution treatment temperature range for maraging steel, due to which even after aging treatment, the microstructure consisted of the partial melt pool characteristics as shown in Fig. 5.4(a) [152].

5.3.2 Wear Behaviour

Grain size of the as-received conventional samples is comparatively larger than those of all other as-built additive samples built in different orientations. Also, due to complex solidification in additive samples, compressive residual stresses remain in the as-built condition, with the result, conventional as-received samples showed high wear rate at each loading condition [29]. The 90^{o} AB samples might have experienced faster heat transfer than those at 45^{o} AB and 0^{o} AB samples respectively which resulted in generation of more residual stresses in 90^{o} AB samples and also the grain size was comparatively smaller. The aforementioned discussion explains the order of wear rate given in Fig. 5.5(a). Similarly, the observed order of wear rate after heat treatment can be explained on the basis of hardness and strength parameters of respective samples presented in Fig. 5.5(b). In the current study, the selected aging temperature falls in the region of over aging and hence, some reverted austenite formation from the martensite matrix can be seen. Austenite is a ductile and softer phase as compared to martensite. The observed order of hardness accordingly varies and depends on volume fraction of reverted austenite as: CM-HT, 0^{o} HT, 90^{o} HT, 45^{o} HT respectively [154]. At lower load (20 N), wear in the samples was due to abrasion and it increased linearly till 40 N load

in both as-built and heat-treated conditions. In as-built samples, beyond applied load of 40 N, the wear rate was retarded and became constant due to strain hardening of contact surfaces at higher loads and change of wear mechanism from abrasive to adhesive. In the case of the HT samples, the overall wear rate was less than that of the as-built samples, at each individual load, due to the improved wear resistance (the hardness was improved by about 40% after heat treatment). Similarly, at relatively low applied load (20 N), the wear was due to abrasion, however, at relatively high load of 80 N, the wear rate was due to adhesion and delamination. On the other hand, after heat treatment, the hard intermetallic phases precipitated acted as facilitators during the wear process and also decreased plastic deformation and tendency of adhesive wear [155]. Due to this reason, the wear rate increased even at higher loads in HT samples as shown in Fig. 5.5(b). The observation of small delamination lamella without significant delamination or wear debris in HT specimen is due to the increased hardness [156].

At lower load of 20N, the hard protruded regions on rotating disc cause ploughing action on the specimen surface, thereby furrow-like features were developed on the surface of the specimen and COF was consequently increased. However, at the higher load of 80N, plastic deformation on the surface of specimen and adhesive wear occurs leading to smoother worn surfaces causing lowering of COF. On comparing COF values of the HT samples with as-built additive and as received conventional samples, it can be concluded that all the HT samples showed lower COF values, which indicates that wear resistance of 18Ni300 maraging steel was improved after heat treatment, in line with the earlier reports. The plot of COF vs time in Fig. 5.6(a, b) reveals fluctuation of coefficient of friction, in the initial period (higher COF). Later after 10-20 Sec, the wear rate and COF showed steady behaviour for all built orientations and heat treatment conditions. There was no significant difference in values of friction coefficient of the as-built and heat-

treated condition, in different orientations of 0°, 45° and 90°. The COF values are consistent with the values reported in literature [156, 33].

5.3.3 Erosion Behaviour

Erosion rate of the as-built (AB) and CM samples was governed by the Meso and microstructure of samples. The conventional samples had coarse equiaxed grains and lower hardness than those found in the as-built samples. Maximum erosion rate was found in these samples. The columnar structure is more prone to erosion as compared to fine cellular grain structure [157]. The semi-elliptical melt pool face consisted of more regions of columnar structure than observed in laser scan face (cellular grains), as shown in Fig. 5.3; thus, the observed order of erosion rate can be understood. After heat treatment, the conventional as well as additive samples, showed martensite structure with little amount of reverted austenite. The 45° HT and CM-HT samples showed maximum erosion rate than the rate in other HT samples. In the CM-HT samples, martensitic lath size and shape are larger than the features observed in HT additive samples. Hence CM-HT samples showed comparatively higher erosion rate. The 45° HT sample, had more reverted austenite phase in its martensite matrix, due to which it showed maximum erosion rate.

5.3.4 Wear and Erosion Surface Morphology

From the analysis of worn surfaces, it can be inferred that there is significant effect of build orientation and load variations on wear behaviour of the materials. Generally, wear testing at low load of 20 N, clearly shows wear tracks and ploughing action. At high applied load of 80 N, the surface of the sample is in contact with the counter disc and leads to delamination and material transfer between mating surfaces [158, 159]. The delamination and material transfer from the surface explains the accelerated wear rate in

the sample at higher loads [160,161]. The clear ploughing and grooves created on wear surface at lower load of 20 N are responsible for higher value of coefficient of friction in the as-built and heat-treated samples (Fig. 5.9). At higher loads, the worn surface showed smooth surface, due to plastic deformation and adhesive wear on surfaces, as a result, the coefficient of friction was reduced. Erosion surface of the as received and heat-treated samples showed ductile erosion consisting of lip, craters, deformed lips as shown in Figs. 5.12 and 5.13. The magnified view of the as-built additive sample showed micro indents and ductile deformed dimples, at higher magnification, clear imprints of preferred columnar structures was observed. The diameter of the nozzle used for erosion was 3mm, as a results shallow erosion depression (~ 600 μm) on metal surface was observed with erodent particles. The microstructural features observed for conventional samples are coarser than the ones depicted by additive samples in both as received and heat treated conditions which led to the formation of more deformed lips and deformation, which can be clearly seen in Figs. 5.12 and 5.13(d). Comparing erosion surface of additive samples in different orientations, it can be inferred that 90^{o} AB samples showed comparatively small deformed lips and crater than those found in 0^{o} AB and 45^{o} AB samples due to comparatively higher hardness. The heat-treated samples showed erosive surfaces similar to surfaces of as-built samples. More deformed lips were observed in 45^{o} HT samples, which might be due to higher percentage of reverted austenite as compared to 90^{o} HT and 0^{o} HT samples.

5. 4. Wear and Erosion Mechanism

After analysing the worn surfaces resulting at different loads and in different conditions, two types of wear mechanisms can be proposed for describing the wear behaviour of M300 maraging steel taken for the present investigation. As discussed earlier, the observed wear behaviour was found to be independent of build orientation and heat

treatment and was dependent only on applied load. At lower load (20 N), clear wear tracks and ploughing wear debris indicate abrasive wear mechanism, as shown in Fig. 5.15(a).

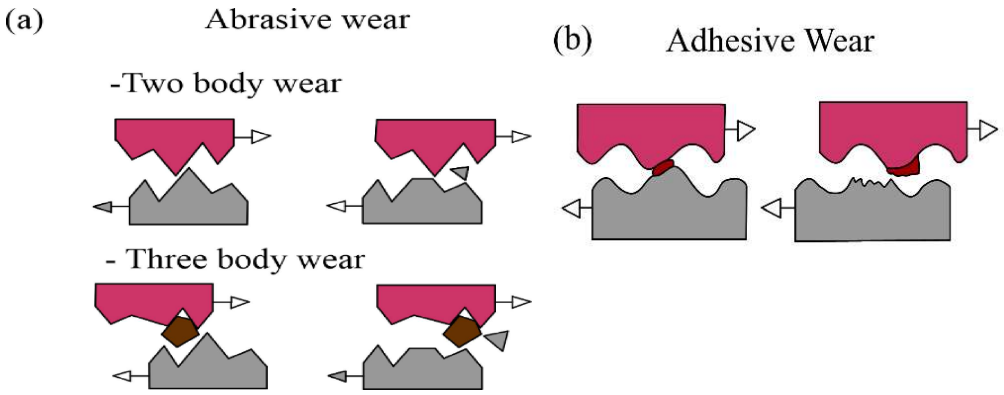

Fig. 5.15 Schematic diagram depicting mechanisms of wear in M300 maraging steel: (a) abrasive wear at 20 N load and (b) adhesive wear at 80 N.

At applied load of 20 N, contacts between the test sample and the disc are similar to tool point contact as the selected disc is harder than the samples, ploughing and clear wear tracks were formed, which is an indication of abrasive wear. On increasing the applied load to 80 N, SEM and AFM images of samples indicate material transfer and delamination which is the characteristics of adhesive wear. In wear testing, at higher applied load on pin, the surface beneath the pin undergoes plastic deformation through tangential frictional force. The contacts between the test samples and rotating disc become surface contacts and materials start sticking, consequently, materials transfer and delamination features are observed on wear surfaces at higher loads. The aforementioned wear mechanism is shown in Fig. 5.15(b). The vertical impingement of erodent particles, on the specimen surface, causes plastic deformation in localized regions and gives rise to lip formation. The repetition of this process causes depression on the surface and gives rise to lips. The fracture of lips by erodent particles results in the formation of small

particles and loss of material on the surface. The aforementioned erosion mechanism is shown in Fig 5.16.

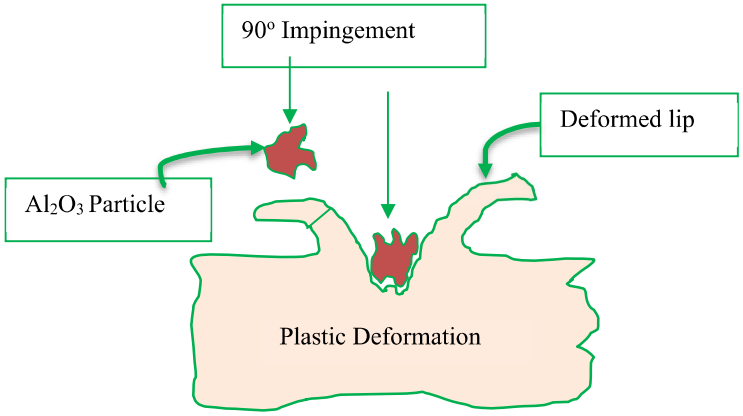

Fig. 5.16 Erosion mechanism of both AM and conventional samples in as received and heat-treated conditions.

5.5 CHAPTER SUMMARY

In the present chapter, a detailed investigation of wear and erosion behaviour of additive manufactured maraging steel built-in 0^o, 45^o and 90^o orientations is carried out and compared with the behavior of conventional samples. The salient observations from this chapter can be summarized as below.

1. Wear rate of samples was affected by applied load. With the increase of load (20 N to 80 N), the wear rate was found to be increased for additive and conventional samples in the as-built, as received and heat treated conditions.

2. In as-built additive samples, wear resistance was dependent on combination of microstructure, residual stresses and hardness whereas after heat treatment, it was mainly governed by precipitation hardening and reverted austenite formed during aging.

3. Microstructure of the as received conventional maraging steel was coarser than those observed in additive samples, hence wear resistance of the as-built additive samples is

superior to the resistance of as received conventional samples. After the heat treatment, due to formation of comparatively lesser percentage of austenite, better wear resistance was seen in conventional samples.

4. COF was found to decrease with increase in load from 20 N to 80 N, due to strain hardening and smoothening of worn surface, as observed from the surface analysis.

5. At lower load (20 N), the mechanism involved for wear was abrasive whereas at higher load, adhesive wear mechanism was dominant.

6. Erosion resistance of sample was governed by meso-structure and microstructure. The conventional sample showed maximum erosion rate due to a comparatively coarser martensitic structure. Erosion surfaces of the as received and heat-treated sample showed ductile erosion, consisting of lips, deformed lips and craters on the eroded surface.